UC Berkeley

Title

Effect of Grain Size on the Ionic Conductivity of a Block Copolymer Electrolyte

Authors

Chintapalli, Mahati
Chen, X Chelsea
Thelen, Jacob L
et al.

Peer reviewed

Effect of Grain Size on the Ionic Conductivity of a Block Copolymer Electrolyte

Mahati Chintapalli,[†,#] X. Chelsea Chen,[#] Jacob L. Thelen,[‡,||] Alexander A. Teran,[‡,||] Xin Wang,[§] Bruce A. Garetz,[§] and Nitash P. Balsara[‡,||,#,*]

[†]Department of Materials Science and Engineering, University of California, Berkeley, California 94720, United States

[‡]Department of Chemical and Biomolecular Engineering, University of California, Berkeley, California 94720, United States

[||]Environmental Energy Technologies Division, Lawrence Berkeley National Laboratory, Berkeley, California 94720, United States

[#]Materials Sciences Division, Lawrence Berkeley National Laboratory, Berkeley, California 94720, United States

[§]Department of Chemical and Biomolecular Engineering, NYU Polytechnic School of Engineering, Brooklyn, New York 11201, United States

S *Supporting Information*

ABSTRACT: A systematic study of the dependence of ionic conductivity on the grain size of a lamellar block copolymer electrolyte was performed. A freeze-dried mixture of poly(styrene)-*block*-poly(ethylene oxide) and lithium bis-(trifluoromethylsulfonyl)imide salt was heated in steps from 29 to 116 °C and then cooled back to 29 °C with an annealing time ranging from 30 to 60 min at each temperature. Grain structure and ionic conductivity during these steps were quantified by *in situ* small-angle X-ray scattering and ac impedance spectroscopy, respectively. Conductivity depends both on grain structure and temperature. A normalization scheme to decouple the dependence of conductivity on temperature and grain structure is described. Ionic conductivity at a given temperature was found to decrease by a factor of 5.2 ± 0.9 as the SAXS measure of grain size increased from 13 to 88 nm. The fact that in the system studied, large, well-formed lamellar grains are less conducting than poorly defined, small grains suggests a new approach for optimizing the transport properties of block copolymer electrolytes. Further work is necessary to confirm the generality of this finding.

1. INTRODUCTION

Block copolymer-based materials are promising candidates for battery electrolytes because the microphase separation of the blocks results in electrolytes with robust mechanical properties and high ionic conductivity, properties that are usually inversely related to each other.[1,2] Solid electrolytes have the potential to eliminate the need for electrode separators and flammable organic liquids that are used in commercial lithium ion batteries today. They may enable the use of lithium metal electrodes in rechargeable batteries by suppressing dendrite growth.[3−5] The block copolymer electrolyte studied in this work is lamellar polystyrene-*block*-poly(ethylene oxide) (PS−PEO or SEO for short), mixed with lithium bis(trifluoromethanesulfonyl)imide (LiTFSI). The PS block is nonconducting and mechanically rigid while the PEO block dissolves LiTSFI and conducts ions. Mixtures of block copolymers and ionic species have been the subject of many studies,[1−3,6−16] due to many unanswered questions related to fundamental polymer physics and the practical need for better rechargeable batteries.

In block copolymers, coherent order is restricted to small regions of characteristic size, L, which we refer to as grains. Figure 1a shows a schematic view of a typical block copolymer electrolyte, which is composed of grains. Here, we show alternating conducting (blue) and nonconducting (red) lamellar domains. In electrolytes created in the absence of external fields, one expects the grains in a macroscopic sample
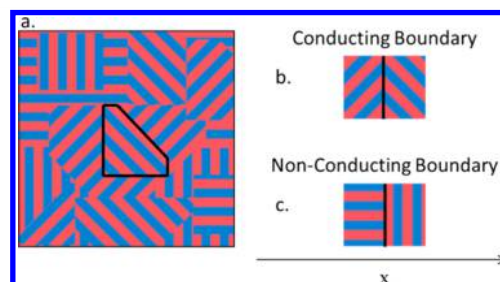

Figure 1. Schematic of a block copolymer electrolyte. In part a, a lamellar block copolymer electrolyte consisting of many grains is illustrated. An example of a grain is outlined in black. The ion conducting domains are blue, and the nonconducting domains are red. In parts b and c, two types of grain boundaries are depicted, one in which ions can travel across the boundary (b), and one in which the ions are blocked by the boundary (c). The *x*-axis indicates the direction of ion transport.

to be randomly oriented, with concomitant defects.[17−24] Ion transport in a collection of grains is more complex than transport within an individual grain, as the former depends on the nature of the defects in addition to the intrinsic material

properties.[8,14] It is customary to use the following expression for the ionic conductivity, σ, of randomly oriented block copolymer grains:

$$\sigma = f\phi_c\sigma_c \tag{1}$$

where ϕ_c is the volume fraction of the conducting block, and σ_c is the intrinsic ionic conductivity of the conductive phase.[1,2,12] The product $\phi_c\sigma_c$ gives the conductivity within each grain, accounting for the presence of the nonconducting microphase. The morphology factor, f, accounts for transport between grains and grain orientation, and, in principle, it can range between zero and one. In Figure 1b,c we have outlined two specific defects that would impact f differently, one that blocks ion transport in the x-direction (Figure 1c) and one that does not (Figure 1b). If the concentration of transport-blocking defects is negligible, then f is $^2/_3$ for a random collection of lamellar grains.[2,25] It is conceivable that the value of f and consequently σ could vary with L due to changes in defect structure with grain size.

The main objective of this paper is to quantify the relationship between conductivity, σ, and average grain size, L, in a block copolymer electrolyte. The grain structure of a block copolymer sample depends on both thermodynamic and kinetic factors. The thermodynamic factors reflect the free energy of defect formation that, in turn, is governed by the orientation of the adjacent grains (tilt versus screw dislocations, etc.).[18,26–28] Upon annealing, defects can annihilate depending on the availability of complementary defects in the neighborhood, as first seen by Harrison et al.[29–31] The distribution of defects in a given sample thus depends not only on the state variables (temperature, pressure, composition) but also on the thermal history. It is thus imperative that in such a study, σ and L are measured simultaneously. We have accomplished this by conducting our experiments in a specially designed air-free X-ray scattering cell that enables *in situ* ac impedance measurements.

2. EXPERIMENTAL SECTION

Electrolyte Preparation. A polystyrene-*block*-poly(ethylene oxide) copolymer was synthesized by living anionic polymerization and characterized by methods described in previous publications.[32–34] The polymer used in this study was found to have a number-averaged molecular weight of 10.4 kg mol^{-1} and a polydispersity of 1.04. The number-averaged molecular weights of the individual blocks were 4.9 kg mol^{-1} for PS and 5.5 kg mol^{-1} for PEO. The block copolymer was mixed with LiTFSI salt (Novolyte) to create the electrolyte. Because of the highly hygroscopic nature of LiTFSI, all operations involving the salt or salt-containing materials were carried out in an Ar glovebox with O_2 and H_2O levels maintained below 1 ppm. The clean SEO was dried for 24 h at 90 °C under vacuum before being introduced into the glovebox. SEO was dissolved in benzene, LiTFSI was dissolved in THF, and the two solutions were stirred for 12 h. In order to make accurate mass measurements to prepare solutions in the dry glovebox environment, a piezoelectric antistatic gun (Milty Zerostat3) was used to treat the area around the glovebox balance to reduce measurement error due to static electricity. The SEO-benzene solution was spiked with salt solution and stirred for 4 h to give an r-value (molar ratio of salt molecules to ethylene oxide moieties) of 0.085. This r-value was chosen because previously SEO electrolytes with r-values in the vicinity of 0.085 have been shown to have optimal ionic conductivities.[12] The dissolved polymer was transferred to a Millrock LD85 lyophilizer without exposure to air and freeze-dried under approximately 1 mTorr of vacuum. The condenser temperature was maintained at −70 °C, and the sample temperature was raised slowly from −70 to 30 °C over the course of 1 week. The electrolyte was then

dried for 24 h in the antechamber of a solvent-free glovebox, under vacuum, at elevated temperature. The amount of water and residual solvent in the electrolyte was found to be below the detection limit of ^{1}H NMR (Figure S1 in the Supporting Information).

Sample Preparation. Samples were prepared for simultaneous characterization by small-angle X-ray scattering (SAXS) and ac impedance spectroscopy. Freeze-dried electrolyte, in the form of a fluffy powder, was mechanically pressed into a fiberglass, Garolite-10 spacer at room temperature to form a transparent, dense pellet. The spacer was 150 μm thick with a hole 3.175 mm in diameter. Two high purity aluminum foils, 17 μm thick and 15.875 mm in diameter, were pressed on either side of the polymer-containing spacer to form electrodes. The thickness of each polymer pellet was determined by measuring the thickness of the electrode and spacer assembly with a micrometer and subtracting the thickness of the electrode foils. Aluminum tabs were attached to the edges of the foil electrodes to make electrical contact without blocking the path for X-rays to travel through the polymer. The samples were vacuum-sealed in a laminated aluminum pouching material (Showa Denko) with the aluminum tabs protruding from the pouch, before being removed from the glovebox. The sample assembly was fixed in place by the 1 atm of pressure acting on the sealed pouch. Blank samples for scattering experiments were made in a similar way, but no polymer was pressed into the spacer and no tabs were attached to the electrodes. After scattering experiments were performed, the samples were disassembled in a glovebox to measure the polymer thickness and inspect the polymer to make sure it did not contain bubbles or macroscopic defects. The difference in sample thickness before and after the annealing experiment was found to be below 10% of the total thickness in all cases.

Small Angle X-ray Scattering. *In situ* small-angle X-ray scattering experiments were conducted at beamline 7.3.3 at the Advanced Light Source in Lawrence Berkeley National Lab (Berkeley, CA) using 10 keV monochromatic X-rays.[35] A Dectris Pilatus 1 M detector with a pixel size of 0.172 mm × 0.172 mm was placed approximately 1.8 m from the sample to image the diffracted X-ray intensity. The distance between the sample and detector and the scattering vector coordinate, q, were determined by calibrating the diffraction images with a silver behenate reference. The magnitude of the scattering vector, q, is given by $q = 4\pi \sin(\theta/2)/\lambda$, where θ is the scattering angle and λ is the wavelength of the X-rays. Three polymer electrolyte samples and one blank sample were mounted onto a home-built temperature-controlled heating stage. All images were obtained using 60 s exposures. Two dimensional scattering data (images) were reduced to one-dimensional intensity, I, versus q profiles by azimuthally averaging using the Nika macro for Igor Pro.[36] For each data point measured, scattering from the blank sample (described above) was subtracted according to eq 2, where I_{Sample} is the raw scattering intensity from the sample, I_{Blank} is the raw scattering intensity of the blank at the corresponding q value, T_{Sample} is the transmission coefficient of the sample, and T_{Blank} is the transmission coefficient of the blank.

$$I = I_{Sample} - \frac{T_{Sample}}{T_{Blank}} \times I_{Blank} \tag{2}$$

The sample transmission coefficient was measured along with every scattering image by recording the total intensity before and after the sample using two ion gauges.

The samples were heated from 29 to 116 °C and cooled back to 29 °C, holding the temperature constant for 30−90 min at each temperature step. The temperature set-point was changed in increments of 5−10 °C during heating and increments of 30 °C during cooling. Several scattering and conductivity measurements were performed for each temperature step. The maximum sample temperature, 116 °C, is well below the degradation temperature of the polymer. The temperature of the heating stage was controlled using a Watlow EZ zone controller and monitored using a thermocouple. At each temperature step during heating, it took approximately 2 min for the stage temperature to reach the set-point. During cooling, which took place passively, it took 15 min to 1 h to reach the set-point. A separate calibration experiment was performed
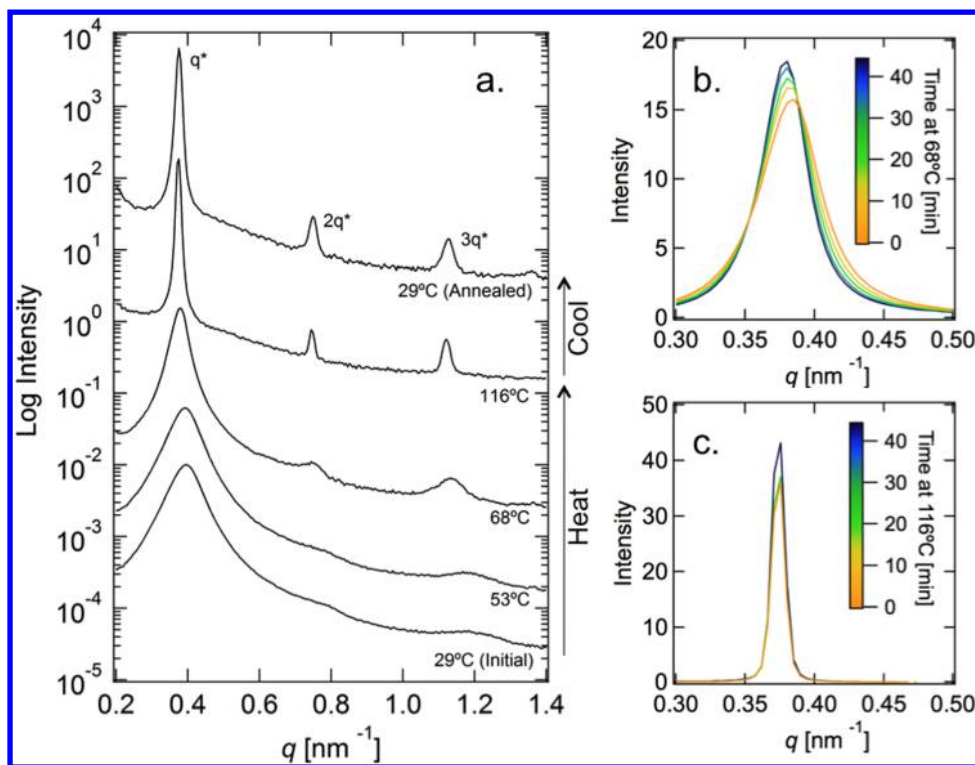
Figure 2. SAXS intensity as a function of the magnitude of the scattering vector, q, during heating and cooling. In part a, SAXS profiles are shown for representative temperatures during heating and cooling, after at least 30 min at each temperature. Profiles are offset for clarity and plotted on a log scale to emphasize the $2q^*$ and $3q^*$ peaks. In parts b and c, the time evolution of profiles is shown at 68 and 116 °C, respectively, plotted on a linear scale.

to relate the stage temperature to the temperature at each sample location; thin wire thermocouples were attached to the samples and the stage was heated to the same temperatures used in the *in situ* experiment (see Figure S3 in the Supporting Information).[37] Temperatures reported herein are sample temperatures (determined via calibration), as opposed to temperature set-points.

Impedance Spectroscopy. The conductivity of the electrolyte in each sample was measured, *in situ*, by performing ac impedance spectroscopy. A Biologic VMP3 potentiostat was connected to the tabs protruding from the pouch to measure the complex impedance as a function of an ac input signal with frequency varying from 1 Hz to 1 MHz and a fixed amplitude of 50 mV. The resistance due to ion transport in the electrolyte was determined from the local minimum in the Nyquist plot of the impedance. The minimum was used to approximate the real axis-intercept, which gives the true resistance. The conductivities of the electrolytes were determined from eq 3, where R_S is resistance, w is the electrolyte thickness, a is the area, and σ is conductivity.

$$\sigma = \frac{w}{R_S a} \tag{3}$$

The inner diameter of the spacer, 3.175 mm, was used to calculate a. For the sample thickness, w, the initial and final thicknesses were averaged.

Transmission Electron Microscopy. Sample structure was verified, *ex situ*, using transmission electron microscopy (TEM). Two bulk samples were prepared using the same procedure for SAXS sample preparation. One was annealed using the same temperature profile, and one was maintained at room temperature, both air-free. Samples were briefly exposed to air to section, stain, and transfer them to the TEM. Thin sections with thicknesses of approximately 100 nm were obtained by cryo-microtoming using a Leica EM FC6 at −120 °C and transferred onto a lacey carbon-coated copper grid (Electron Microscopy Sciences). Samples were stained in RuO_4 vapor for 10 min. Scanning transmission electron microscopy (STEM) experiments

were performed on a Tecnai F20 UT FEG equipped with a high angle annular dark field (HAADF) detector using 200 keV acceleration voltage. PEO domains appear bright in images.[38,39]

3. RESULTS AND DISCUSSION

Simultaneous SAXS and conductivity measurements were performed for three independent samples. Conductivity measurements (without SAXS) were performed on six additional independent samples. All of the results obtained from these experiments were consistent with each other. Because of our interest in studying the dependence of ionic conductivity on grain size and because grain size is known to be a sensitive function of thermal history,[40] we only discuss the results of the simultaneous SAXS and conductivity experiments. For clarity, we begin our discussion by describing one of the samples.

Figure 2a shows selected SAXS profiles obtained at representative temperatures between 29 and 116 °C. All of the profiles contain a prominent primary scattering peak in the vicinity of $q = q^* \approx 0.38$ nm^{-1} and higher order peaks at $2q^*$ and $3q^*$, indicating that the block copolymer morphology is lamellar over the entire temperature window. The primary and higher order peaks obtained from the as-prepared, freeze-dried sample are broad. Increasing sample temperature above 63 °C results in a decrease in the widths of primary and higher order peaks (heating data in Figure 2a). At a given temperature, peak width decreases with annealing time, albeit at a rate that is highly temperature dependent. This is illustrated in Figure 2b,c, where data collected over a 40 min time interval at 68 and 116 °C are shown. Changes in peak width with time are more readily seen at 68 °C.

The SAXS peak widths are affected primarily by variation in domain spacing and finite grain size. We assume that the variation in domain spacing arises from the polydispersity in the polymer sample and is thus independent of temperature and annealing history. The dependence of peak width on temperature and annealing history is assumed to arise from changes in the average grain size. As expected, the average grain size increases irreversibly with annealing. Cooling the sample from 116 to 29 °C has virtually no effect on peak width (Figure 2a). The SAXS profiles obtained at 116 °C are essentially independent of time, except for data obtained at 33 min (Figure 2c). We do not know the reason for the outlier. In addition to peak width, the value of q^* also changes irreversibly, as documented in the Supporting Information (Figure S4). In our analysis of morphology, we focus on changes in the full width at half-maximum (fwhm) of the primary peak and ignore changes in q^*. The validity of our approach is confirmed by TEM. Electron micrographs of an as-prepared freeze-dried sample and a sample annealed from 29 to 116 °C are shown in Figure 3. The average size of the coherently ordered grains in the freeze-dried sample is much smaller than that in the annealed sample. A variety of distinct defe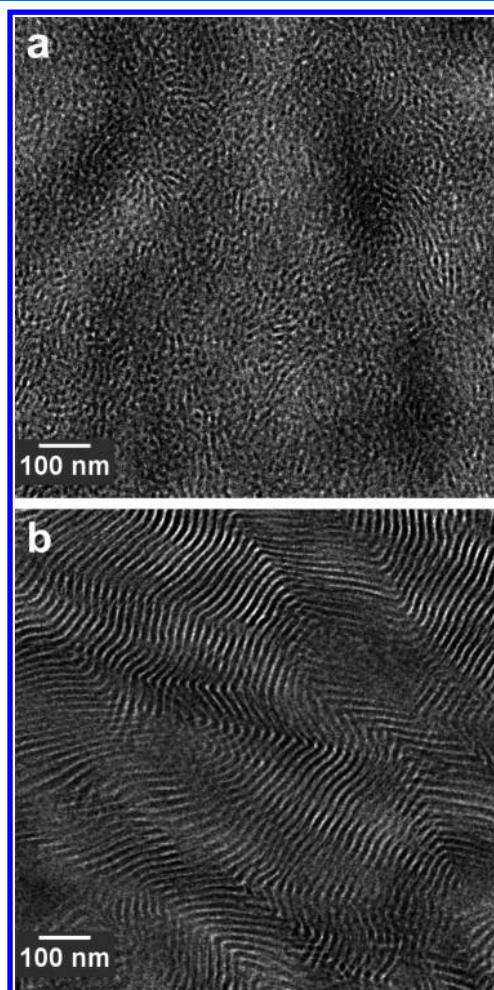ct structures including low and high angle tilts (v patterns) and twists (x patterns) are discernible in the annealed sample (Figure 3b). The geometries of the defects in the freeze-dried sample are less clear (Figure 3a).

The fwhm of the primary SAXS peak of each scattering profile was determined in two steps. First, the SAXS peak intensity was calculated by subtracting a linear baseline, fit in the vicinity of the primary peak. Second, linear interpolation between the two data points closest to the half-maximum, on each side of the scattering peak, was used to determine fwhm. Grain size, L, is approximated by $L \approx \mathrm{fwhm}^{-1}$, based on the Scherrer equation. Typical samples contain grains of a distribution of shapes and sizes, and the relationship between L as defined here and the average grain size determined by other approaches such as quantitative analysis of TEM images[30] or depolarized light scattering[41] is unclear. In Figure 4, the

Figure 3. STEM images of electrolyte samples before and after annealing. In part a, the electrolyte was cold pressed after freeze-drying, and in part b, the electrolyte was freeze-dried, cold pressed, and then annealed from 29 to 116 °C before cooling to room temperature. The samples were stained with RuO_4, and images were obtained using an HAADF detector. PEO domains appear bright.
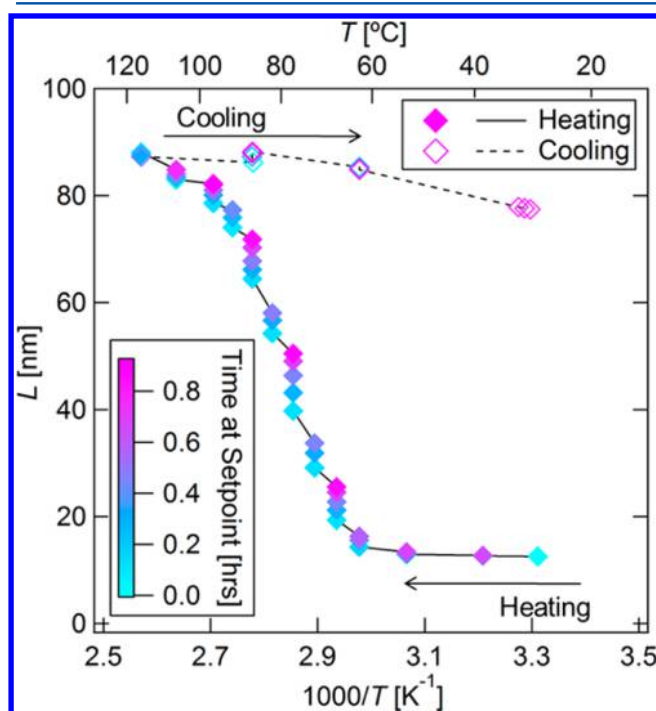

Figure 4. Dependence of grain size, L, on temperature, T. The grain size is plotted as a function of temperature with the color scale indicating the amount of time the sample spent at a given temperature. Lines are drawn to guide the eye.

average grain size, L, determined by SAXS is plotted against inverse temperature. Inverse temperature is used for ease of comparison with conductivity data, which is generally plotted using the same abscissa (the top abscissa in Figure 4 shows sample temperature in °C). Heating the sample from 29 to 63 °C has very little effect on L. The value of L in this regime, 13 nm, is comparable to the domain spacing (16.5 nm), indicating a highly disordered morphology. As the temperature is increased beyond 63 °C, the grain size begins to grow with time and temperature. The average grain size is a much weaker function of temperature during the cooling run (Figure 4). Cooling the electrolyte below this temperature results in only a slight decrease in L. The SAXS data in Figure 4 are in excellent agreement with the TEM images in Figure 3.

In Figure 5a, we show the observed grain growth as a function of time, t, at selected temperatures. The ordinate in Figure 5a is L/L_0 where L_0 is the grain size at $t = 0$ for a given temperature. The temperature dependence of L_0 is given in
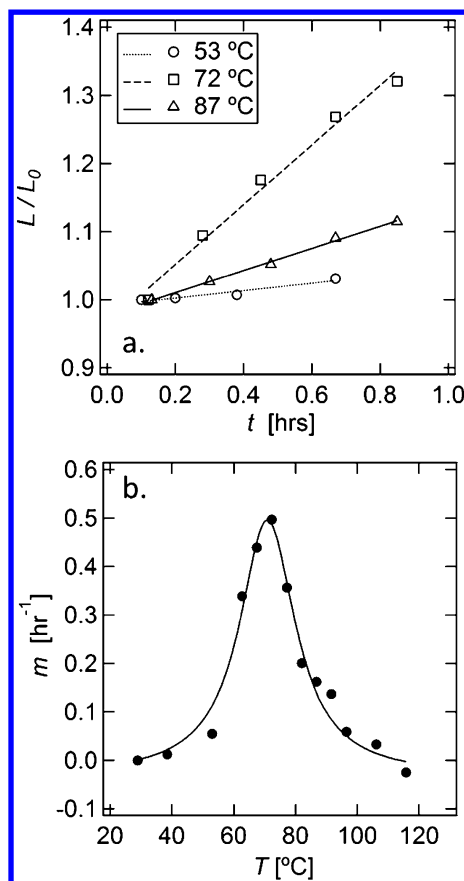
Figure 5. Grain growth as a function of temperature. In part a, dimensionless grain size is plotted against time for three representative temperatures during sample heating. Linear fits through the data are shown. In part b, the grain growth rate, determined from the slope of the fits in part a, is plotted as a function of temperature. A line is drawn to guide the eye.

Figure 4 ($t = 0$ h data during the heating run). The slope of the linear fit through each data series in Figure 5a gives the history-dependent nondimensional grain growth rate, m, defined as $m = \mathrm{d}(L/L_0)/\mathrm{d}t$, at the temperature of interest. It is worth noting that the grain growth is approximately linear in the time window of our experiment. One expects power law behavior or saturation at long times.[17] At 53 °C, L/L_0 increases slowly with time with a growth rate of 0.055 h^{-1}. Increasing the temperature to 68 °C results in a much larger growth rate of 0.44 h^{-1}. Increasing the temperature to 87 °C results in a significant slow-down of growth rate, and a value of 0.16 h^{-1} is obtained. Figure 5b shows the temperature dependence of m observed during the annealing process. The largest growth rate occurs around 72 °C, which is very close to 71 °C, the glass transition temperature of PS, the structural block, ($T_{\mathrm{g,PS}}$; see Figure S2 in the Supporting Information for differential scanning calorimetry data). The as-prepared, freeze-dried sample contains a high concentration of defects. At temperatures lower than $T_{\mathrm{g,PS}}$, chain mobility is limited, and this limits defect annihilation. In the vicinity of $T_{\mathrm{g,PS}}$, the chains have sufficient mobility, and the most unstable defects are rapidly consumed. We posit that the normalized grain growth rate decreases beyond 72 °C because the remaining defects are more stable (lower free energy) and their concentration is lower. Ryu et al. have shown that annealing block copolymers results in the preferential elimination of certain kinds of

defects.[30] This may be related to the free energy of defect formation as calculated by Matsen et al.[42] In addition, the barrier for defect annihilation, which will depend on defect concentration, will play an important role in the dependence of grain growth rate on temperature. It is evident that m depends on L_0 (which is inversely related to defect density) and T. As anticipated in the introduction, the grain structure of our sample is dependent on both the temperature of the system and on the thermal history.

In addition to scattering (data shown in Figures 2 and 4), conductivity was also monitored with time and temperature. In Figure 6, conductivity data is shown for the same representative
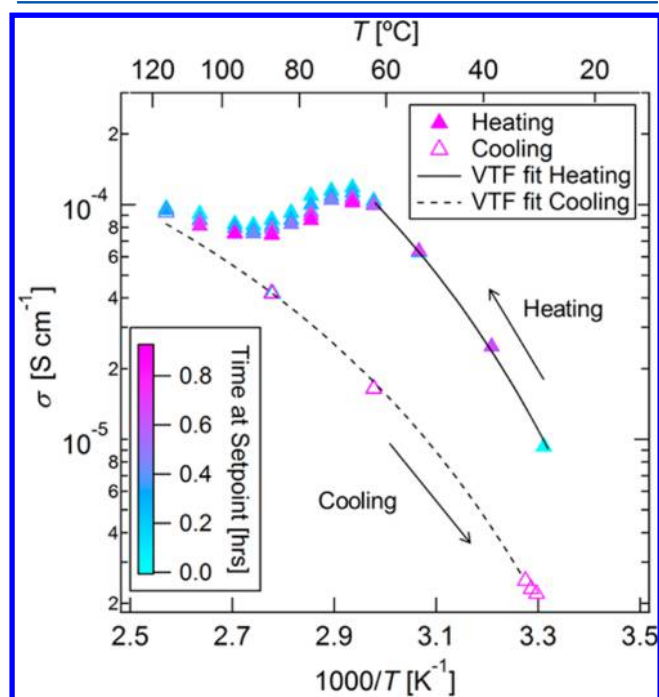

Figure 6. Conductivity as a function of temperature and time. Conductivity data are shown for a representative sample during heating (filled triangles) and cooling (open triangles). Heating data below 68 °C and all of the cooling data are both fit to the VTF model (solid and dashed curves). The color scale represents the time spent at each temperature.

sample discussed in Figures 2−5. Upon heating, at temperatures between 29 and 63 °C, the conductivity increases with temperature but does not change significantly with time. When the sample is heated from 53 to 63 °C, the conductivity first increases and then decreases with increasing time. Each subsequent step along the heating curve results in the same qualitative behavior: a discontinuous increase in conductivity at early times followed by a decrease in conductivity at longer times. After completing the last heating step from 106 to 116 °C, the sample was cooled in steps as shown in Figure 6. Data obtained at different temperatures during the cooling run were independent of time; the open symbols in Figure 6 representing cooling data are superpositions of several conductivity measurements as a function of time at each temperature.

There are two regimes wherein the grain structure is a relatively weak function of temperature: (1) during the heating run between 29 and 63 °C and (2) during the cooling run between 116 and 29 °C (see Figure 4). We use the term "stable grain structure" to describe the sample during these two

regimes as it is clear that grain growth does not occur in spite of rapid molecular motion. The Vogel–Tammann–Fulcher (VTF) model is often used to describe ionic conductivity in homogeneous polymer systems or heterogeneous polymer systems with fixed microstructure.[1,43] We use the VTF equation to fit conductivity obtained in the two regimes described above:

$$\sigma_{VTF}(T) = AT^{-1/2} \exp\left(\frac{-E_a}{R(T - T_0)}\right) \tag{4}$$

In eq 4, $\sigma_{VTF}(T)$ is the VTF fit to the conductivity as a function of temperature, A is a prefactor that, in theory, is related to the number of charge carriers, E_a is the effective activation energy for ion transport, R is the gas constant, and T_0 is a reference temperature. In all VTF fits used in this study, T_0 was taken to be −40 °C, which is the glass transition temperature of the ion-conducting block, PEO. The parameters E_a and A obtained from the fits are shown in Table 1. In addition, we also show

Table 1. Vogel–Tammann–Fulcher Parameters for Conductivity Dependence on Temperature During Sample Heating and Cooling

condition	E_a [kJ mol^{-1}]	A [S cm^{-1} K$^{1/2}$]	σ_{120} [S cm^{-1}]
heating	4.3 ± 0.1	0.35 ± 0.09	$7 \times 10^{-4} \pm 1 \times 10^{-4}$
cooling	4.3 ± 0.2	0.07 ± 0.03	$1.4 \times 10^{-4} \pm 0.4 \times 10^{-4}$
heating/ cooling (unitless)	0.99 ± 0.03	5.2 ± 1.3	5.2 ± 0.9

σ_{120}, which is the conductivity at 120 °C predicted by the VTF fit. The quantities reported in Table 1 represent the average and standard deviation of the values for three independent samples studied simultaneously by SAXS and ac impedance.

The VTF parameters are given for the fit to the stable grain structure during the heating and the cooling run. The value of each fit at 120 °C is given in the last column. The last row gives the dimensionless ratio of the parameters obtained during the heating run to those obtained during the cooling run. The values represent the average and standard deviation of parameters for three separate samples

The VTF parameters obtained during heating represent conductivity through the as-prepared, freeze-dried sample with small grains, while the VTF parameters obtained during cooling represent conductivity through the well-annealed, large grains. Comparing the conductivities of these two systems at fixed temperature (e.g., 120 °C) enables quantification of the effect of grain structure on ion transport. It is evident that increasing L from 13 to 88 nm (Figure 4) results in a decrease in conductivity by a factor of 5.2 (Table 1). It is perhaps interesting to note that the activation energies obtained during heating and cooling are within experimental error (Table 1). The change in conductivity is mainly due to a difference in the prefactor A (Table 1). In homogeneous electrolytes, it is normally assumed that the magnitude of A reflects the concentration of charge carriers. One, however, does not expect the grain size to affect the number of charge carriers. We are thus not sure of the origin of the observed relationship between L and A.

In Figure 7, we establish an explicit relationship between conductivity and structure by plotting the conductivity against grain size. In Figure 7a, raw conductivity, σ, obtained during heating is plotted against grain size for the representative
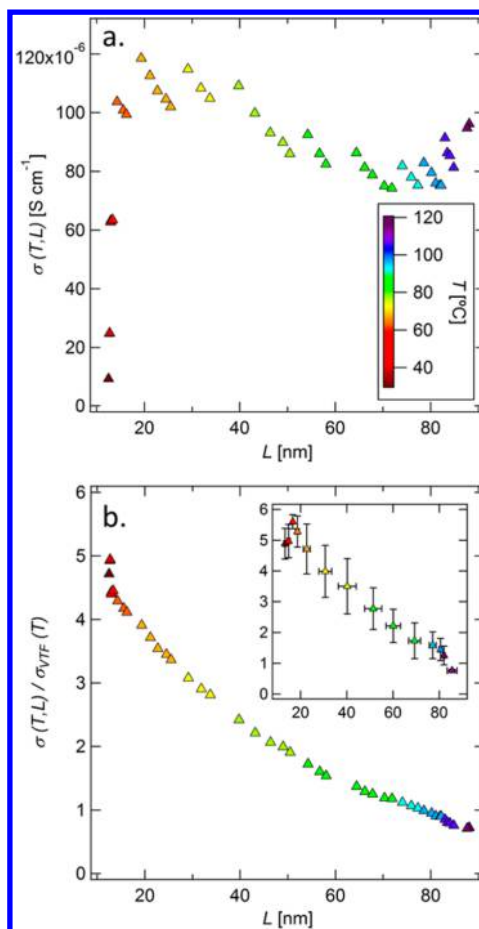

Figure 7. Dependence of conductivity on grain size. In part a, raw conductivity of a representative sample is plotted against grain size, and in part b, normalized conductivity is plotted. The color scale represents the temperature at each data point for both plots. The inset in part b shows normalized conductivity data averaged for three samples. The vertical and horizontal error bars represent one standard deviation in each direction.

sample used in the previous figures. This σ vs L plot does not reveal a clear relationship because σ depends on both L and T. To isolate the dependence of σ on L, the raw conductivity was normalized by the VTF fit to the cooling data. This serves as a reference conductivity corresponding to the stable grain structure of the well-annealed sample. In Figure 7b, normalized conductivity, σ/σ_{VTF} is plotted against L, and a clear relationship is revealed between the two. Normalized conductivity data from three samples studied simultaneously by SAXS and ac impedance were binned into groups of five adjacent data points and averaged. The averaged data is shown in the inset in Figure 7b, with error bars representing one standard deviation in each direction. It is important to note that the trends seen in Figure 7b would also be obtained if we were to use the VTF fit through the conductivity data obtained from the stable grains obtained during the heating run because the E_a value is similar and T_0 is identical. The values of σ/σ_{VTF} would be reduced by a factor of about five due to differences in A between the heating and cooling fits (see Figure S5 in the Supporting Information).

We can use eq 1 to study the effect of increasing L on the morphology factor, f, for the three samples used in the simultaneous SAXS and ac impedance experiments. In order to

do this, we need estimates of σ_c and ϕ_c. On the basis of the characterization data given above, we assume $\phi_c = 0.58$ (independent of temperature). To estimate σ_c, a straightforward approach is to assume that σ_c is equal to the conductivity of a mixture of PEO homopolymer and LiTFSI at $r = 0.085$ (the same value as for the block copolymer).[13] The conductivity of PEO/LiTFSI mixtures at $r = 0.085$ is independent of homopolymer molecular weight when it exceeds about 5 kg mol^{-1}.[44] As discussed in previous publications,[45] obtaining pure PEO microphases by self-assembly of block copolymers requires strong segregation, which, in the case of symmetric SEO copolymers, occurs when the total molecular weight of the copolymer exceeds 100 kg mol^{-1}. The SEO used in this study (4.9 kg mol^{-1} PS and 5.5 kg mol^{-1} PEO) is clearly not in this regime. Since the extent of mixing of PS segments in the PEO-rich microphases has not been measured directly, we use the conductivity of PEO/LiTFSI at a given temperature to estimate σ_c. To quantify the effect of L on f, conductivity measurements obtained at 63 °C (heating run) and at 65 °C (cooling run) were used. At 63 °C, $\sigma_c = 5.95 \times 10^{-4}$ S cm^{-1}, and at 65 °C, $\sigma_c = 6.55 \times 10^{-4}$ S cm^{-1}. Values of σ_c were calculated at the temperatures of interest based on the published work of Yuan et al.[13] and Teran et al.[44] During heating, at 63 °C, when the samples are composed of small grains ($L = 13$ nm), we obtain $f = 0.36 \pm 0.05$, and during cooling, at 65 °C, when the samples are composed of large grains ($L = 88$ nm), $f = 0.058 \pm 0.013$. The values of f reported here are the average and standard deviation of the f values for the three samples. Increasing L causes f to decrease. The value of f in both regimes is considerably smaller than the ideal value of 0.67 for lamellar structures due to the aforementioned mixing of glassy PS segments in the PEO-rich microphases.[13,15]

It is clear from Figure 7b that conductivity decreases as grain size increases. This result indicates that poor long-range order is desirable in block copolymer electrolytes. It also sheds light on previously published data on the effect of molecular weight on the conductivity of block copolymer electrolytes; increasing molecular weight resulted in an increase in conductivity.[12,13] We expect defect annihilation to slow down with increasing molecular weight. Trapped defects and small grain sizes may be one of the reasons why high molecular weight block copolymer electrolytes exhibit high conductivities. The passage of ions through defective lamellar phases of the kind pictured in Figure 3 is nontrivial, and we have not identified the particular defects in the well-annealed sample (Figure 3b) that impede ion motion. It is conceivable that annealing block copolymers results selectively in the formation of defects pictured in Figure 1c, which in turn reduce ionic conductivity.

4. CONCLUSIONS

We have performed a systematic study of the influence of grain size on the ionic conductivity of a lamellar block copolymer electrolyte. As the electrolyte was heated in steps from 29 to 116 °C, the grain size increased with time and temperature, with a maximum in the normalized grain growth rate in the vicinity of the T_g of the structural block, PS. After the heating run was complete, a stable structural state was reached, and the grain structure did not change appreciably when the polymer was cooled. The dependence of the conductivity on temperature followed VTF behavior in temperature regimes where the structure did not change significantly; however, when grain size increased, conductivity decreased in all cases. Typically, it is difficult to deconvolute the effects of microstructure and

temperature on conductivity because the three quantities are interrelated, and because microstructure and measured conductivity of the block copolymer are both history-dependent. By normalizing the conductivity with the conductivity in a reference state with constant microstructure, the grain size-dependence of the conductivity was isolated. It was observed that conductivity decreases with increasing grain size. This study points to long-range order as a parameter that should be considered when designing block copolymer electrolytes. All other characteristics being equal, block copolymers with small grains are better electrolytes than those with larger, well-defined grains. It is possible that in other block copolymer systems, the kinetics of grain growth and the types of grain boundaries formed upon annealing may not be the same as in this system. More work is needed to confirm the generality of the finding that large grains impede conductivity. The fact that the poorly defined lamellae pictured in Figure 3a are five times more conductive than the clearly defined lamellae in Figure 3b may, at first, appear counterintuitive. We hope to identify the underpinnings of this surprising observation in future studies.

■ ASSOCIATED CONTENT

Ⓢ Supporting Information

Electrolyte characterization, temperature calibration, the dependence of domain spacing on temperature, and normalization of conductivity by the VTF fit to heating data. This material is available free of charge via the Internet at http://pubs.acs.org.

■ AUTHOR INFORMATION

Corresponding Author

*E-mail: nbalsara@berkeley.edu.

Author Contributions

The manuscript was written through contributions of all authors. All authors have given approval to the final version of the manuscript.

Notes

The authors declare no competing financial interest.

■ ACKNOWLEDGMENTS

ABBREVIATIONS

PS	polystyrene
PEO	poly(ethylene oxide)
SEO	polystyrene-*block*-poly(ethylene oxide)
LiTFSI	lithium bis(trifluoromethanesulfonyl) imide
L	grain size (nm)
σ	ionic conductivity (S cm^{-1})
ϕ_v	volume fraction of conducting block
σ_c	homopolymer ionic conductivity (S cm^{-1})
f	morphology factor
r	ratio of salt molecules to PEO monomers
SAXS	small-angle X-ray scattering
q	scattering vector magnitude (nm^{-1})
λ	wavelength of X-rays (nm)
θ	scattering angle
I, I_{Sample}, I_{Blank}	intensities
T_{Sample}, T_{Blank}	transmission coefficients
R_S	resistance (Ω)
w	length (cm)
a	area (cm^2)
q^*	primary scattering peak coordinate (nm^{-1})
fwhm	full width at half-maximum of scattering peak (nm^{-1})
L_0	initial grain size (nm)
m	history-dependent nondimensional grain growth rate
$T_{g,PS}$	glass transition temperature of polystyrene (°C)
VTF	Vogel−Tammann−Fulcher model
σ_{VTF}	ionic conductivity from VTF model (S cm^{-1})
A	VTF prefactor (S cm^{-1} K$^{1/2}$)
T	temperature (°C)
T_0	reference temperature (°C)
E_a	activation energy (kJ mol^{-1})
R	gas constant (J mol^{-1} K^{-1})
σ_{120}	value of VTF fit at 120 °C

REFERENCES

(1) Young, W. S.; Kuan, W. F.; Epps, T. H. *J. Polym. Sci., Part B: Polym. Phys.* **2014**, *52*, 1−16.

(2) Singh, M.; Odusanya, O.; Wilmes, G. M.; Eitouni, H. B.; Gomez, E. D.; Patel, A. J.; Chen, V. L.; Park, M. J.; Fragouli, P.; Iatrou, H.; Hadjichristidis, N.; Cookson, D.; Sciences, M.; Di, V.; Berkeley, L. *Macromolecules* **2007**, *40*, 4578−4585.

(3) Bouchet, R.; Maria, S.; Meziane, R.; Aboulaich, A.; Lienafa, L.; Bonnet, J.; Phan, T. N. T.; Bertin, D.; Gigmes, D.; Devaux, D.; Denoyel, R.; Armand, M. *Nat. Mater.* **2013**, *12*, 452−457.

(4) Stone, G. M.; Mullin, S. A.; Teran, A. A.; Hallinan, D. T.; Minor, A. M.; Hexemer, A.; Balsara, N. P. *J. Electrochem. Soc.* **2012**, *159*, A222−A227.

(5) Monroe, C.; Newman, J. *J. Electrochem. Soc.* **2003**, *150*, A1377.

(6) Simone, P. M.; Lodge, T. P. *ACS Appl. Mater. Interfaces* **2009**, *1*, 2812−2820.

(7) Weber, R. L.; Ye, Y.; Schmitt, A. L.; Banik, S. M.; Elabd, Y. A.; Mahanthappa, M. K. *Macromolecules* **2011**, *44*, 5727−5735.

(8) Young, W. S.; Epps, T. H. *Macromolecules* **2012**, *45*, 4689−4697.

(9) Young, W. S.; Epps, T. H. *Macromolecules* **2009**, *42*, 2672−2678.

(10) Zhang, S.; Lee, K. H.; Sun, J.; Frisbie, C. D.; Lodge, T. P. *Macromolecules* **2011**, *44*, 8981−8989.

(11) Mullin, S. A.; Stone, G. M.; Panday, A.; Balsara, N. P. *J. Electrochem. Soc.* **2011**, *158*, A619.

(12) Panday, A.; Mullin, S.; Gomez, E. D.; Wanakule, N.; Chen, V. L.; Hexemer, A.; Pople, J.; Balsara, N. P. *Macromolecules* **2009**, *42*, 4632−4637.

(13) Yuan, R.; Teran, A. A.; Gurevitch, I.; Mullin, S. A.; Wanakule, N. S.; Balsara, N. P. *Macromolecules* **2013**, *46*, 914−921.

(14) Kim, S. H.; Misner, M. J.; Yang, L.; Gang, O.; Ocko, B. M.; Russell, T. P. *Macromolecules* **2006**, *39*, 8473−8479.

(15) Bouchet, R.; Phan, T. N. T.; Beaudoin, E.; Devaux, D.; Davidson, P.; Bertin, D.; Denoyel, R. *Macromolecules* **2014**, *47*, 2659−2665.

(16) Mullin, S. A.; Stone, G. M.; Teran, A. A.; Hallinan, D. T.; Hexemer, A.; Balsara, N. P. *Nano Lett.* **2012**, *12*, 464−468.

(17) Dai, H.; Balsara, N.; Garetz, B.; Newstein, M. *Phys. Rev. Lett.* **1996**, *77*, 3677−3680.

(18) Gido, S. P.; Gunther, J.; Thomas, E. L.; Hoffman, D. *Macromolecules* **1993**, *26*, 4506−4520.

(19) Gido, S. P.; Thomas, E. L. *Macromolecules* **1994**, *27*, 849−861.

(20) Gido, S. P.; Thomas, E. L. *Macromolecules* **1997**, *30*, 3739−3746.

(21) Gido, S. P.; Thomas, E. L. *Macromolecules* **1994**, *27*, 6137−6144.

(22) Chastek, T. Q.; Lodge, T. P. *J. Polym. Sci., Part B: Polym. Phys.* **2005**, *43*, 405−412.

(23) Hashimoto, T.; Nagatoshi, K.; Kawai, H.; October, R. *Macromolecules* **1974**, *7*, 364−373.

(24) Nishikawa, Y.; Kawada, H.; Hasegawa, H.; Hashimoto, T. *Acta Polym.* **1993**, *44*, 247−255.

(25) Sax, J.; Ottino, J. M. *Polym. Eng. Sci.* **1983**, *23*, 165−176.

(26) Netz, R.; Andelman, D.; Schick, M. *Phys. Rev. Lett.* **1997**, *79*, 1058−1061.

(27) Ryu, H. J.; Fortner, D. B.; Rohrer, G. S.; Bockstaller, M. R. *Phys. Rev. Lett.* **2012**, *108*, 107801.

(28) Matsen, M. W. *J. Chem. Phys.* **1997**, *107*, 8110−8119.

(29) Harrison, C.; Adamson, D. H.; Cheng, Z.; Sebastian, J. M.; Sethuraman, S.; Huse, D. A.; Register, R. A.; Chaikan, P. M. *Science* **2000**, *290*, 1558−1560.

(30) Ryu, H. J.; Fortner, D. B.; Lee, S.; Ferebee, R.; De Graef, M.; Misichronis, K.; Avgeropoulos, A.; Bockstaller, M. R. *Macromolecules* **2013**, *46*, 204−215.

(31) Huang, E.; Mansky, P.; Russell, T. P.; Harrison, C.; Chaikin, P. M.; Register, R. A.; Hawker, C. J.; Mays, J. *Macromolecules* **2000**, *33*, 80−88.

(32) Teran, A. A.; Balsara, N. P. *J. Phys. Chem. B* **2014**, *118*, 4−17.

(33) Hadjichristidis, N.; Iatrou, H.; Pispas, S.; Pitsikalis, M. *J. Polym. Sci., Part A: Polym. Chem.* **2000**, *38*, 3211−3234.

(34) Quirk, R. P.; Kim, J.; Kausch, C.; Chun, M. *Polym. Int.* **1996**, *39*, 3−10.

(35) Hexemer, A.; Bras, W.; Glossinger, J.; Schaible, E.; Gann, E.; Kirian, R.; MacDowell, A.; Church, M.; Rude, B.; Padmore, H. *J. Phys. Conf. Ser.* **2010**, *247*, 012007.

(36) Ilavsky, J. *J. Appl. Crystallogr.* **2012**, *45*, 324−328.

(37) Thelen, J. L.; Teran, A. A.; Wang, X.; Garetz, B. A.; Nakamura, I.; Wang, Z.; Balsara, N. P. *Macromolecules* **2014**, *47*, 2666−2673.

(38) Huang, P.; Zhu, L.; Cheng, S. Z. D.; Ge, Q.; Quirk, R. P.; Thomas, E. L.; Lotz, B.; Hsiao, B. S.; Liu, L.; Yeh, F. *Macromolecules* **2001**, *34*, 6649−6657.

(39) Trent, J. S.; Scheinbeim, J. I.; Couchman, P. R. *Macromolecules* **1983**, *16*, 589−598.

(40) Kim, W. G.; Chang, M. Y.; Garetz, B. A.; Newstein, M. C.; Balsara, N. P.; Lee, J. H.; Hahn, H.; Patel, S. S. *J. Chem. Phys.* **2001**, *114*, 10196.

(41) Balsara, N. P.; Garetz, B. A.; Dai, H. J. *Macromolecules* **1992**, *25*, 6072−6074.

(42) Matsen, M. W. *J. Chem. Phys.* **1997**, *107*, 8110−8119.

(43) Lascaud, S.; Perrier, M.; Vallke, A.; Besner, S.; Prud, J.; Armand, M. *Macromolecules* **1994**, *27*, 7469−7477.

(44) Teran, A. A.; Tang, M. H.; Mullin, S. A.; Balsara, N. P. *Solid State Ionics* **2011**, *203*, 18−21.

(45) Ozcam, A. E.; Petzetakis, N.; Silverman, S.; Jha, A. K.; Balsara, N. P. *Macromolecules* **2013**, *46*, 9652−9658.